Biosensors and Bioelectronics 46 (2013) 15–21

Contents lists available at SciVerse ScienceDirect

Biosensors and Bioelectronics

journal homepage: www.elsevier.com/locate/bios

Label-free biosensor based on an electrical tracing-assisted silicon microring resonator with a low-cost broadband source

Kyung Woo Kim [a], Junfeng Song [a,b], Jack Sheng Kee [a], Qing Liu [a], Guo-Qiang Lo [a], Mi Kyoung Park [a,*]

[a] Institute of Microelectronics, A*STAR (Agency for Science, Technology and Research), 11 Science Park Road, Singapore Science Park II, Singapore 117685, Singapore

[b] State Key Laboratory on Integrated Opto-Electronics, College of Electronic Science and Engineering, Jilin University, Changchun 130023, China

ARTICLE INFO

Article history:
Received 1 October 2012
Received in revised form
25 January 2013
Accepted 2 February 2013
Available online 26 February 2013

Keywords:
Silicon microring resonator
Electrical-tracing
Cost-effective light source
Label-free biosensor
HER2 detection

ABSTRACT

We present a novel biosensor based on an electrical tracing-assisted silicon dual-microring resonator sensor system. The dual-microring system comprises one microring resonator as a sensing element and the other microring resonator integrated with an electrical controller as a tracing element. The resonance wavelength shift of the sensing microring induced by the refractive index change due to antigen–ligand bindings is traced and determined by direct voltage applied to the electrical tunable tracing microring. The sensor system enables the use of a low-cost broadband light source instead of a bulky and expensive tunable laser, which allows the development of cost-effective point-of-care diagnostic devices by significantly reducing the device cost and increasing its portability. The sensing capability of the developed dual-microring sensor was investigated using biotin–streptavidin binding as a model system. We have demonstrated the quantitative detection of streptavidin over a broad range of concentrations down to 190 pM by monitoring the electrical power applied to the tracing ring. We have also validated the sensing principle of the dual-microring system by a direct comparison between the calculated and measured values for the resonance wavelength shift of the sensing microring. Furthermore, we have shown the quantitative and specific detection of a well-known breast cancer biomarker, human epidermal growth factor receptor 2 (HER2), in a bovine serum albumin solution using the antibody-modified dual-microring sensor system.

1. Introduction

The application of biosensors in medical diagnostics has several advantages over other diagnostic methods, including reduced assay time, non-invasiveness, flexibility, multi-target analysis, automation, and reduced cost of testing (Rasooly and Jacobson, 2006). One of the most promising applications of biosensor technology is point-of-care (POC) diagnosis. POC systems can allow medical staff and patients to get clinical outcomes easily and rapidly beyond hospitals and research centres and have a potential to reduce medical expense (Bohunicky and Mousa, 2011). Successful development of POC technologies will provide better screening of at-risk patients, tighter surveillance of disease recurrence, and better monitoring of treatment (Soper et al., 2006).

Recently, silicon-on-insulator (SOI) microring resonator-based biosensors have gained significant attention because of their high sensitivity, extremely small footprint, and low fabrication costs due to their complementary metal oxide semiconductor (CMOS) capability (Park et al., 2013). They can be integrated into a compact array, provide highly multiplexed detection within a single device, and can be readily combined with fluidic components. To date, silicon microring resonator-based biosensors have demonstrated highly sensitive, label-free, and real-time detection of proteins (De Vos et al., 2007; Washburn et al., 2009, 2010; Iqbal et al., 2010; Park et al., 2013), nucleic acids (Qavi et al., 2010, 2011a, 2011b; Scheler et al., 2012), lectins (Kirk et al., 2011), and viruses (McClellan et al., 2012). However, although sensor chips can be made as cheap disposable devices, an expensive and bulky high-resolution wavelength-tunable laser is required to accurately measure the resonance wavelength shift. Thus, the detection limit is ultimately restricted by the laser resolution. Therefore, biosensors based on conventional microring resonators may not be suitable for cost-effective POC application.

Recently, we reported a proof-of-principle of a novel electrical tracing-assisted dual-microring system that enables the use of an inexpensive broadband light source. The dual-microring system comprises an array of microring resonators as a sensing element

* Corresponding author. Tel.: +65 6770 7522; fax: +65 6778 0136.
E-mail address: parkmk@ime.a-star.edu.sg (M.K. Park).

0956-5663/$ - see front matter © 2013 Elsevier B.V. All rights reserved.
http://dx.doi.org/10.1016/j.bios.2013.02.002

and a thermo-optically tunable modulator as a tracing element (Song et al., 2012). In this device, the resonance wavelength shift of the sensing microring induced by the index change due to antigen–ligand bindings is traced and determined by direct voltage supplies to the electrical tunable tracing microring. In this work, we investigate the biosensing capability of the dual-microring device using the biotin–streptavidin system as a model. We also demonstrate the specific detection of the well-known breast cancer biomarker human epidermal growth factor receptor 2 (HER2) using an anti-HER2 antibody-modified sensor. This report establishes the novel dual-microring system as a promising cost-effective diagnostic device by significantly reducing the device cost and increasing its portability while taking full advantage of the intrinsic properties of a silicon microring sensor, such as highly sensitive, label-free, and multiplexed detection.

2. Material and methods

2.1. Materials

(3-N-((6-(*N*′-isopropylidiene-hydrazino)-nicotinamide)propyl-triethoxysilane) (HyNic-Silane), succinimidyl-4-formylbenzamide (S-4FB) and anhydrous dimethylformamide (DMF) were purchased from SoluLink (San Diego, CA, USA). Recombinant human receptor tyrosine-protein kinase (ErbB2, also known as HER2) (M.W.= 71 kDa) and rabbit polyclonal antibody to recombinant human ErbB2 were purchased from Sino Biological Inc. (Beijing, China). 3-aminopropyltriethoxysilane (APTES), bovine serum albumin (BSA), poly (sodium-4-styrenesulfonate) (PSS), and poly (allylamine hydrochloride) (PAH) were purchased from Sigma-Aldrich (St. Louis, MO, USA). Immunopure streptavidin and EZ-Link NHS-PE4-biotin were purchased from Thermo Scientific Pierce (Singapore). Other chemicals were analytical reagent grade and were used as received. All samples and buffers were prepared using deionized (DI) water obtained from a Milli-Q water purification system.

2.2. Sensing principle

Fig. 1 shows the working principle and schematic of the dual-ring resonator sensing system, which comprises two serially cascaded microring resonators. The first microring senses the effective index change near the ring surface (*sensing ring*), while the second microring traces the resonance wavelength shift of the sensing ring by means of a microheater that can be controlled by applying the electrical power (*tracing ring*). For the tracing ring, the resonance wavelength shift ($\Delta\lambda_t$) according to the applied electrical power (ΔW) can be expressed as

$$\Delta\lambda_t = A\Delta W = 2AV\Delta V/R \quad (1)$$

where A is the thermo-optic coefficient, V is applied voltage, and R is the heater resistance (Song et al., 2012).

A broadband light that is coupled into an input-port goes through the sensing microring and feeds into the tracing microring from a drop-port of the sensing microring. If we limit the wavelength range of the broadband light source to be less than the free-spectral range (FSR), there is only one resonance for each microring. The output intensity from the output-port reaches maximum only when both resonances align with each other, according to the filter-cascading effect. Without applying any electrical power, the resonance peaks from the sensing ring (λ_s) and the tracing ring (λ_t) are separate from each other; therefore, the output power would be at the minimum. By scanning the electrical power applied to the tracing microring while monitoring the output intensity, the required electrical power for the tracing ring to align with the sensing ring ($W_1(\lambda_s-\lambda_t)$) can be obtained (Fig. 1(a)). Then, when the antigen binds with the antibody attached on the sensing ring surface, the resonance wavelength of the sensing ring shifts due to the index change. Therefore, the electrical power required for the tracing ring to align with the sensing ring shifts accordingly ($W_2(\lambda_{s'}-\lambda_t)$) (Fig. 1(b)). The resonance wavelength shift of the sensing ring can thus be indirectly extracted by monitoring the power change of the tracing ring, which can be expressed as

$$\Delta W(\Delta\lambda_s) = W_2(\lambda_{s'}-\lambda_t) - W_1(\lambda_s-\lambda_t) \quad (2)$$

2.3. Fabrication and characterization

Fig. 2(a) shows the layout design of the dual-ring resonator-based optical sensor system. The sensing system has three input ports and three output ports in order to measure the optical

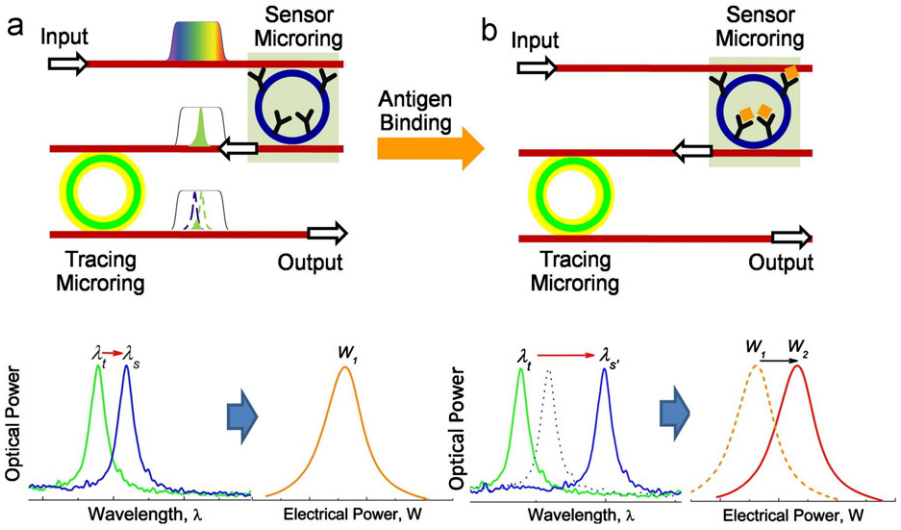

Fig. 1. Schematic of the electrical tracing-assisted dual-microring resonator optical sensor system, which adopts two serial cascaded add-drop microring resonators. Biomolecule binding events (i.e., antibody–antigen interaction) on the surface microring lead to an increase in the effective refractive index and a shift in the resonance wavelength. (a) Before antigen binding; the tracing microring requires electrical power $W_1(\lambda_s-\lambda_t)$ in order to trace and align the resonances with those of the sensing microring. (b) After antigen binding; the resonance shift of the sensing microring due to the refractive index change requires $W_2(\lambda_{s'}-\lambda_t)$ electrical power for the tracing microring to trace and align with the shifted resonance. The $\Delta\lambda_s$ can be extracted from the electrical power change of $W_2(\lambda_{s'}-\lambda_t)-W_1(\lambda_s-\lambda_t)$.

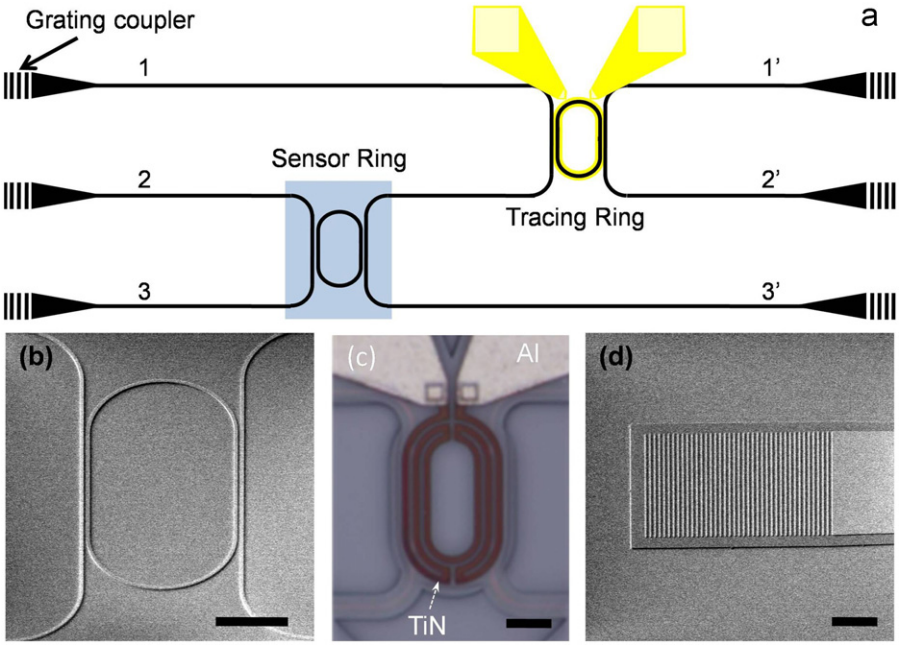

Fig. 2. (a) Layout design of the dual-microring-based sensing system. A grating coupler is located at each end of a linear waveguide for vertical light coupling. (b) SEM image of race-track style microring as a sensing ring, (c) optical image of a tracing ring integrated with thermal heater, and (d) SEM image of a grating coupler.

properties of each microring separately. Unlike the previous device with end-fire coupling that used an inverse taper (which has better coupling loss but poor tolerance), grating couplers for vertical coupling are used instead for the current device. The vertical grating coupling method allows higher alignment tolerance, which is an important factor in designing cartridge-based sensors (Zimmermann et al., 2008). From transmission 1–1′ and 3–3′, we can separately measure the drop-port optical responses of the tracing ring and the sensing ring. From 2 to 2′, we can measure the optical power from the dual-ring sensing system. The rings are race-track style rings with a radius of 10 μm and a coupling length of 20 μm. A typical SEM image of a microring is shown in Fig. 2(b). The waveguide dimensions are 500 nm × 220 nm and the gap between the linear waveguide and the ring is 350 nm. A grating coupler (20 μm width, Λ=630 nm, etch depth=70 nm, filling factor=0.5, N=40) is connected to a linear waveguide via an adiabatic taper (from 20 μm wide to 500 nm wide, 200 μm length) (Taillaert et al., 2006). A SEM image is shown in Fig. 2(d).

The fabrication process is similar to that of a thermo-optic switch (Song et al., 2008, 2011). We started the fabrication on a commercially available 200 mm SOI wafer with a 220 nm-thick top silicon layer and a 2 μm-thick buried oxide (BOX) layer. First, the microring structure is patterned using 248-nm deep UV lithography and etched to the BOX using the reactive ion etching (RIE) process. Then 1.5 μm of high-density plasma (HDP) oxide is deposited, followed by 150 nm titanium nitride (TiN) deposition for the thermal heater. Both the width and the gap of the heater strip are 1.5 μm. Next, 30 nm-thick silicon nitride is deposited for TiN etching protection. After the formation of contact holes, ~750 nm thick aluminum is deposited, followed by metal pad etching. Finally, the sensing window is opened for the sensing microring using a RIE dry etch process. Fig. 2(c) shows an optical image of the fabricated tracing microring.

2.4. Polyelectrolyte multilayer deposition

The silicon microring device was first treated with oxygen plasma. It was then immersed in a solution of 2% APTES in a mixture of ethanol/H_2O (95%/5%, v/v) for 2 h, followed by thorough rinsing with ethanol and DI water. It was then dried under a nitrogen stream and heated at 120 °C for 15 min. A polyelectrolyte multilayer film was built by alternately immersing the device in aqueous solutions of PSS (1.0 mg/mL in 50 mM NaCl) and PAH (1.0 mg/mL in 50 mM NaCl) for 15 min each. After each polymer deposition, the device was rinsed three times in DI water and dried with nitrogen.

2.5. Biotin–streptavidin binding

The sensor surface was first functionalized with APTES, as described in the previous section. The sensor chip was then incubated with 1 mg/mL NHS-biotin in DI water for 1 h and rinsed with DI water. The binding assay between biotin and streptavidin was performed by applying streptavidin solution in PBS (190 pM–950 nM). For flow control, acrylic wells designed for the attachment of Tygon tubes were adhered onto the surface of the silicon chips prior to the binding assay (Chua et al., 2009). The volume of liquid in the solution chamber was 15 μL. Liquid flow was controlled by a peristaltic pump (Watson Marlow 401U/DM3, Falmouth, UK). All experiments were carried out at room temperature.

2.6. Antibody immobilization and protein detection

Covalent attachment of antibodies to the sensor surface was accomplished using hydrazone-bond-formation chemistry based on the formation of a covalent bond formed between an aromatic hydrazine and an aromatic aldehyde (Byeon et al., 2010). The sensor chip was first treated with oxygen plasma. It was then immersed in a solution of 1 mg/mL HyNic silane in 95% ethanol and 5% DMF for 30 min, followed by thorough rinsing with ethanol. It was then dried under a nitrogen stream.

A solution containing 100 μg of polyclonal anti-HER2 was buffer exchanged into a modification buffer (100 mM sodium phosphate, 150 mM sodium chloride, pH 7.4) using a Zeba desalt column. A 10-fold molar excess of 20 mg/mL S-4FB solution in anhydrous DMF was added to the antibody solution (~0.43 mg/mL) and the

reaction mixture was allowed to incubate for 2 h on a shaker. Following the incubation, excess 4-FB was removed and buffer exchanged into a conjugation buffer (100 mM sodium phosphate, 150 mM sodium chloride, pH 6.0) using a Zeba desalt column. An antibody-immobilized surface was then prepared by flowing the S-4FB-modified antibody solution (100 μg/mL) over the HyNic-modified sensor surface at a rate of 8.5 μL/min for 1 h. The sensor was passivated with 1% BSA in PBS for 20 min, followed by washing with the same buffer.

The binding assay between the immobilized antibody and HER2 protein was performed by applying solutions containing recombinant human HER2 (140 nM in 20 mM HEPES buffer). To evaluate the specificity of the interaction, the change in applied voltage of a high concentration of BSA in HEPES buffer (0.1 wt%, 15 μM) was investigated.

2.7. Optical setup

Details of the optical setup and procedure to measure the dual-ring system have been described in a previous paper (Song et al., 2012). In short, the C-band amplified spontaneous emission (ASE) light source (Opto-Link Corp. Ltd., Hong Kong) and the band-pass tunable filter (Alnair Labs, BVF-200, Tokyo, Japan) are used as a wide-band light source. An erbium doped fiber amplifier (EDFA) is used to boost optical power. The polarization controller is used to control the polarization of the input light (TE-mode). The light is coupled from the polarization-maintaining single mode fiber to the grating coupler. The output light is also coupled from a grating coupler to another single mode fiber and detected using an optical power meter. The power meter (Agilent 81634B, Santa Clara, CA, USA) and the power supplier (Agilent E3641A, Santa Clara, CA, USA) are remotely controlled through a computer interface developed in our laboratory using the LabVIEW program. The optical power reading was recorded while sweeping applied voltage over a given range, and an applied voltage value at the maximum optical power was recorded in realtime using the LabVIEW program. The optical spectrum was measured using an optical spectrum analyzer (OSA, Agilent 86142B).

3. Results and discussion

3.1. Dual-microring device characterization

The thermal tuning capability of the tracing ring was first investigated by monitoring the shift in the 1–1′ transmission spectra of the tracing microring upon a voltage change from 0.0 V to 5.0 V (0.5 V stepwise). The transmission spectra are normalized to a waveguide transmission at 0.0 V. A typical tracing ring has a free-spectral range (FSR) of 5.64 nm and a Q-factor of 4000. As the voltage applied to the metal heater increased, the temperature of the tracing ring rose, thus resulting in a red-shift in the resonance wavelength of the microring (Fig. 3(a)). The power consumption according to the applied voltage can be calculated based on the measured electrical resistance (~890 Ω, see supplements Fig. S1) using $W=V^2/R$. The linear fit of the measured resonance positions as a function of the applied electrical power shows the thermal tuning efficiency of 0.14 ± 0.01 nm/mW ($R^2=0.999$, 7.1 ± 0.5 mW/nm; 7.1 mW is needed to tune the resonance wavelength shift by 1 nm) (Fig. 3(b)). The variance for the efficiency of tracing rings across the entire wafer was found to be 10 pm/mW, which is within the measurement device's noise level. Compared to our previous device (Song et al., 2012), the thermal tuning efficiency has improved by 40% (0.1 nm/mW vs. 0.14 nm/mW), which will be advantageous for a battery operated hand-held diagnostic device that requires lower power consumption.

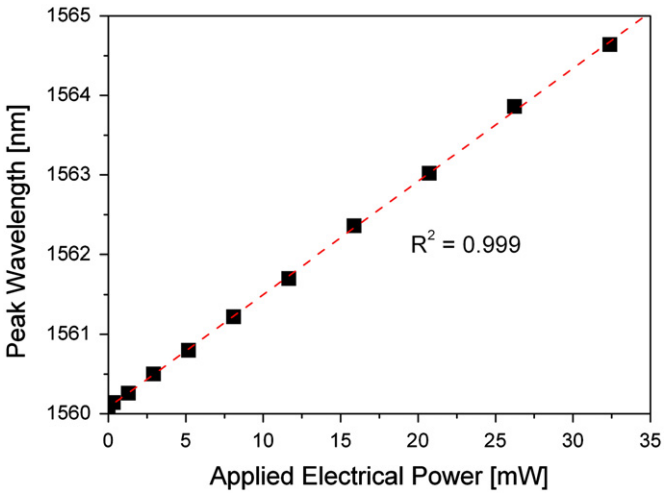

Fig. 3. (a) Measured transmission spectra of the tracing ring upon different DC voltages. (b) Resonance wavelength peak positions as a function of the applied electrical powers. Linear fitting shows the thermal tuning efficiency of ~0.14 nm/mW. (For interpretation of the references to color in this figure legend, the reader is referred to the web version of this article.)

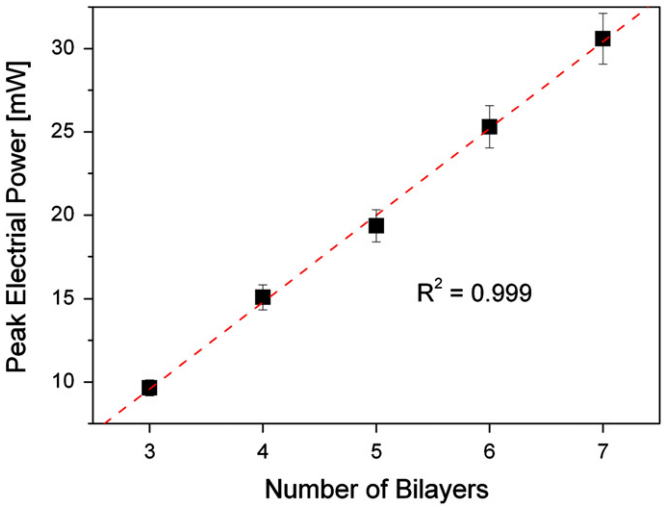

Fig. 4. The applied electrical power versus the number of bilayers (n) after the deposition of $(PSS/PAH)_n$. The measurement was taken in air.

The surface senstivity of the dual-microring was investigated using the deposition of a polyelectroltye multilayer, which is known to have well-controlled and reproducible thicknesses (Bertrand et al., 2000). The 2–2′ transmission was measured while scanning the electrical power applied to the tracing ring with the broadband input light. The optical response of the sensing ring according to scanning the electrical power upon the number of deposited PSS/PAH bilayers (supplements Fig. S2). Therefore, the required electrical power for the tracing microring to trace and align with the sensing ring's resonance peak increased. The applied electrical power versus the number of deposited bilayers is shown in Fig. 4. The linear fitting shows that the change of applied electrical power for each PSS/PAH bilayer is 5.20 ± 0.3 mW ($R^2=0.999$). The sensitivity for surface mass (S_m)

detection is given by:

$$S_m = \Delta W/\sigma_p, \quad (3)$$

where σ_p is the surface density of a polymer layer and ΔW is the applied electrical power. As the mass density of the polyelectrolyte multilayer was known to be 1.2×10^6 g/m^3 (Caruso et al., 1997; Park et al., 2013), the surface density was calculated to be $\sim$2.0 ng/mm^2 for each PSS/PAH bilayer. Using the value of the applied electrical power from this experiment, we can calculate the mass sensitivity of $S_m = 2.6 \pm 0.1$ mW/ng/m^2. The detection limit of a sensor is defined by:

$$L_m = R/S_m, \quad (4)$$

where R is the sensor resolution related to the system noise. The resolution of the dual-microring system can be estimated from $R = 3\sigma$, where σ is the total system noise. The DC power supply used in the current investigation has an accuracy of 0.1% ($\pm$5 mV). Depending on the operating voltage for each sensor, the resolution of the dual-microring system is within the range of 90–160 μW (operation voltage of 2.5–4.5 V). Therefore, the detection limit of $L_m = 34 - 62 \pm 4$ pg/mm^2 was calculated using Eq. (4). Since high system noise is mainly caused by the accuracy of the DC power supply, we are currently working on developing a power supply with a noise level < 1 mV which can be incorporated into a hand-held system for the next generation. This will significantly reduce the total system resolution and therefore improve the system's detection limit.

3.2. Biotin–streptavidin binding

To demonstrate the biosensing capability of the dual-ring system, a well-characterized biotin–streptavidin interaction was used as a model system. The interaction between biotin and streptavidin is one of the highest non-covalent affinities ($K_D = 10^{-13}$ M) and is therefore stable and specific (Pérez-Luna et al., 1999; Jung et al., 2000). The sensor surface was functionalized with biotin and a solution of streptavidin in PBS was flowed over the sensors at a rate of 8.5 μL/min for a total duration of 60 min. This was followed by washing with PBS to remove unbound streptavidin. The 2–2′ transmission with the broadband source was measured while scanning the applied electrical power to the tracing ring. Fig. 5(a) shows the applied electrical power (ΔW) of a biotin-modified sensor to trace the shift in the sensing ring's resonance peak ($\Delta\lambda_s$) as a function of the concentration of streptavidin solution ranging from 0.19 nM to 0.95 μM. ΔW gradually increased as the concentration of streptavidin increased and finally reached the saturation level (3.2 ± 0.2 mW) and was linear on the log–log scale within the concentration range of the experiments ($R^2 = 0.9727$). Error bars indicate the standard deviation of the measured electrical powers among different chips. The lowest concentration used in the experiment was 0.19 nM, causing a 0.12 mW shift. In order to confirm the measurements using the electrical tracing technique, the calculated $\Delta\lambda$ from ΔW using the thermal efficiency of the tracing ring (0.14 ± 0.01 nm/mW) was compared to the measured $\Delta\lambda$ using an optical spectrum analyzer (Table 1). The resonance wavelength shift from the 2 to 2′ transmission after streptavidin binding was obtained using the optical spectrum analyzer. Since the resolution of the spectrum analyzer is 60 pm, there is a degree of discrepancy between the calculated values and the measured values for low concentrations of streptavidin. However, for the high concentration range, the measured $\Delta\lambda$ value is consistent with the calculated $\Delta\lambda$, which confirms the sensing principle of the electrical tracing-assisted sensing system.

The binding affinity and cooperative effects during streptavidin recognition were investigated using the Hill plot (Fig. 5(b)). The Hill equation for this interaction is described as follows (Pathirana et al., 2000):

$$\log\left[\frac{Y}{1-Y}\right] = n\log[\mathrm{Str}] - \log(K_D), \quad (5)$$

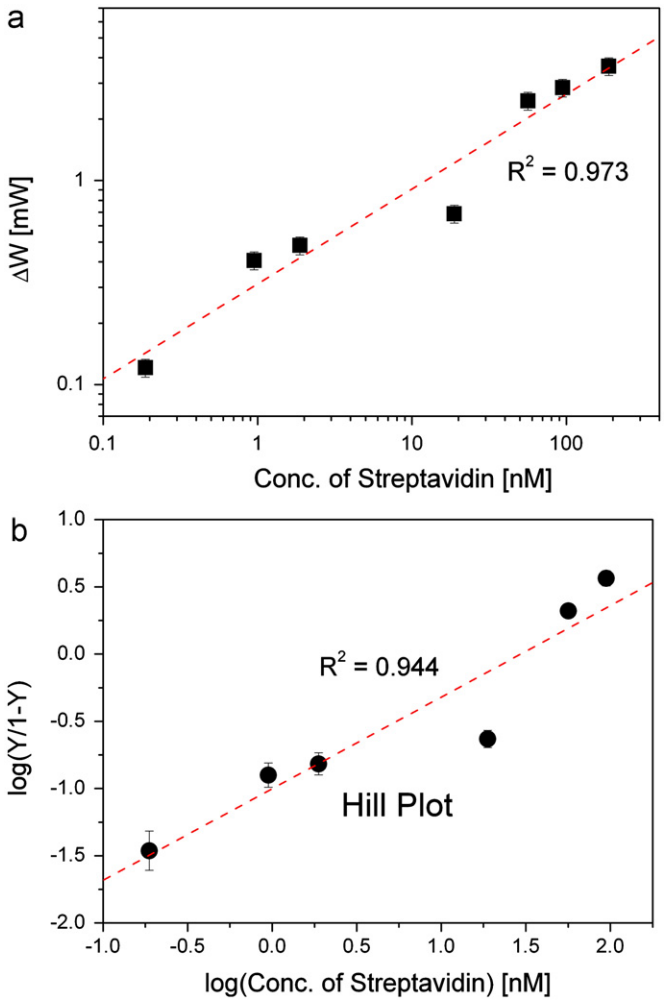

Fig. 5. (a) Binding curve for the detection of streptavidin using a biotin-modified dual-microring sensor. The applied electrical power versus different concentrations of streptavidin solution is plotted in log–log scale. (b) A Hill plot. The ration of occupied and free biotins is shown as a function of the concentration of streptavidin. The linear line represents the least square fit of Eq. (5) with coefficients $K_D = 1.0 \times 10^{-9}$ M and $n = 0.68$ ($R^2 = 0.944$).

Table 1
Comparison between calculated $\Delta\lambda$ from the applied electrical power for the tracing ring and directly measured $\Delta\lambda$.

Concentration (nM)	$\Delta W \pm$ SD[a] (mW)	$\Delta\lambda$, Calculated (pm)[b]	$\Delta\lambda$, Measured (pm)[c]
0.19	0.12 ± 0.01	17 ± 2	–
0.95	0.41 ± 0.02	57 ± 2	40
1.9	0.48 ± 0.03	67 ± 3	50
19	0.73 ± 0.04	102 ± 5	100
56	2.46 ± 0.13	344 ± 17	350
95	2.85 ± 0.14	399 ± 19	400
950	3.15 ± 0.15	440 ± 22	450

[a] Standard deviation.
[b] Calculated from the thermal efficiency of the tracing ring ($\Delta\lambda = 0.14$ nm/mW $\times \Delta W$).
[c] Measured one time using an optical spectrum analyzer. The resolution of the analyzer is 60 pm.

where $Y/1-Y$ is the ratio of the occupied biotin molecules to the unbound biotin on the sensing surface, $Y=\Delta W/\Delta W_{max}$, n is the Hill coefficient, [Str] is the concentration of free streptavidin solution, and K_D is the dissociation constant. From the fitting, the dissociation constant K_D is 1.0 (± 0.1) $\times 10^{-9}$ M and $n=0.68$ ($R^2=0.944$). The data indicate that streptavidin binding to immobilized biotin molecules is characterized by a negative cooperativity ($n<1$), which indicates that more than one binding site (immobilized biotins) is needed to bind one streptavidin molecule. This is consistent with the binding mechanisms of streptavidin binding to surface-bound biotins where a single streptavidin link (monovalent) and double-bounded streptavidin (immobilized via two surface biotins) coexist (Jung et al., 2000). Although the dissociation constant (K_D) between streptavidin and biotin in a solution is typically extremely high (10^{-13} M), the dissociation constant between streptavidin and surface-bound biotin varies in the published data, which is in the nano- to pico-molar range in most cases, depending on the experimental conditions and methodologies (Encarnação et al., 2009). The obtained K_D value in Fig. 5(b) is within the same order of magnitude as previous data from quartz crystal microbalance (QCM) based on impedance analysis (Encarnação et al., 2009) and ELISA assays (Chilkoti et al., 1995). The dissociation constant of the current system can be further optimized by controlling the surface density of surface-bound biotins. It has been shown that a dilution of the surface-bound biotins is necessary to reduce steric hindrance between streptavidin molecules (Spinke et al., 1993).

3.3. Anti-HER2 immobilization and HER2 binding

The sensing capability of the dual-ring sensor was further investigated using a well-known breast cancer biomarker, HER2. HER2 is a cancer antigen that can be measured as an indicator for normal biologic processes, pathogenic processes, or pharmacologic responses to therapeutic intervention. HER2 is amplified and/or overexpressed in approximately 20–25% of invasive breast cancers (Esteva et al., 2005). For the sensitive detection of biomolecules, it is important to develop a robust method to immobilize capture ligands, such as antibodies. In this work, we used chemoselective hydrazone-bond-formation chemistry (Byeon et al., 2010). The sensor surface was first treated with HyNic silane, resulting in a hydrazine-terminated surface. Next, antibodies tagged with S-4FB were added to the surface to form a covalent bond between the hydrazine-terminated surface and aryl aldehydes on the antibodies via hydrazone bond formation. Fig. 6 shows the real-time response of the HyNic silane-modified sensor upon the addition of the anti-HER2 antibody modified with S-4FB and followed by washing with a buffer solution. The applied electrical power (ΔW) after the antibody immobilization was determined to be 2.04 mW, which corresponded to the 286 pm spectral shift of the sensing ring. This is similar to the previous literature values of 260–280 pm measured by a conventional microring sensor (Washburn et al., 2009). The sensor surface was then treated with 0.1% BSA solution in order to block the non-specific binding site.

After the immobilization of anti-HER2 antibodies, the sensor was tested to verify that the sensors were responsive to HER2 protein binding. The binding curves of different concentrations of HER2 protein ranging from 70 nM to 1.4 μM are shown in Fig. 7(a). The real-time response of the sensor was recorded while HER2 solution was flowed over the sensor at a rate of 8.5 μL/min. Between the experiments, the surface was then regenerated by injecting a glycine buffer (50 mM, pH 2.6) at a rate of 23 μL/min for 2 min. Upon the exposure to HER2, the required electrical power rapidly increased, which indicates an increase in the effective index on the sensor surface resulting from the binding

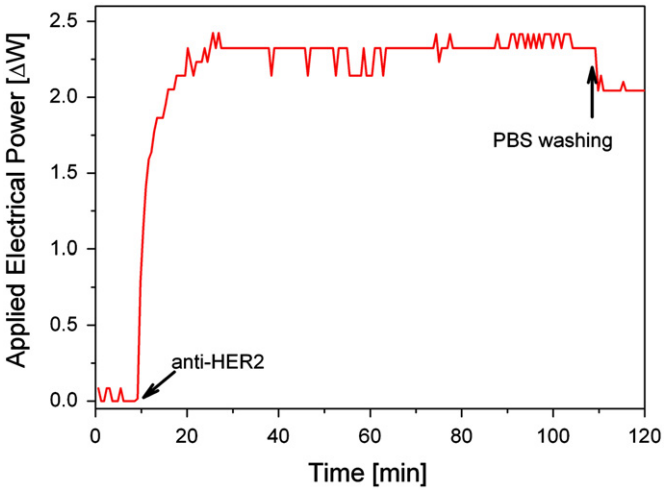

Fig. 6. Real-time monitoring of the shift in applied electrical power during covalent immobilization of the anti-HER2 antibody on the microring sensor surface.

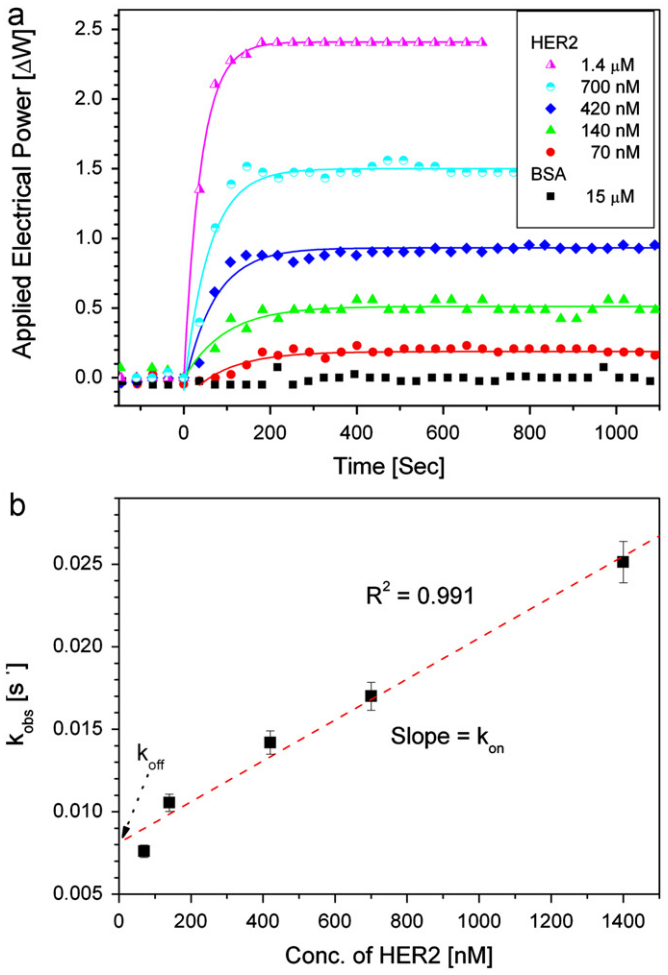

Fig. 7. (a) The biding curve of the applied electrical power using the anti-HER2 antibody functionalized microring upon exposure from 70 nM to 1.4 μM of HER2 solution in an HEPES buffer. The high concentration of BSA (0.1%, 15 μM) on the anti-HER2 antibody-modified sensor surface is shown as a control. (b) The observed association rate constant against the concentration of HER2, k_{obs}, is obtained and plotted based on the binding curve for each concentration.

of HER2 molecules to their antibodies on the sensor surface. The electrical power typically reached saturation after 10 min of binding. For one-to-one binding between antibody and antigen,

the observed association rate constant, k_{obs}, is defined as follows (Lin et al., 2006):

$$k_{obs} = k_b + k_a[\text{HER2}], \quad (6)$$

where k_a is the association rate constant, k_b is the dissociation rate constant, and [HER2] is the concentration of HER2 protein in HEPES buffer. The binding curve for each concentration was fitted using Origin and the obtained k_{obs} was plotted against the concentration of HER2 (Fig. 7(b)). Using the slope and the intercept from the linear fit, ka and k_b were obtained to be 1.24 $(\pm 0.06)\times 10^4\ \text{M}^{-1}/\text{s}$ and 8.12 $(\pm 0.42)\times 10^{-3}\ \text{s}^{-1}$ (R^2=0.991), respectively. Using these values, the dissociation constant, $K_D = k_b/k_a$ was calculated to be 6.55 $(\pm 0.35)\times 10^{-7}$ M, which is within same magnitude of order with the previous literature value measured by opto-fluidic ring resonator (Gohring et al., 2010). Non-specific binding was confirmed by applying a high concentration of BSA (0.1%, 15 μM) to the anti-HER2 antibody-modified sensor surface. Even after 20 min, there was no significant shift in the resonance wavelength (Fig. 7(a)). In addition, 0.1 wt% BSA was added to HEPES as a binding buffer for the HER2 solution in order to demonstrate the specificity of the sensor. A comparison between HER2 binding with and without the presence of BSA did not show significant changes in the applied electrical power (supplements Fig. S3). Furthermore, the responses from different sensor chips after repeated glycine buffer regeneration with 140 nM of HER2 binding were investigated to examine the uniformity of sensors as well as the consistency of sensor response before and after regeneration process and the data showed that the variability is within 19.1% (supplements Fig. S4).

4. Conclusions

Recently, silicon microring resonators have been used in many bio-sensing applications, leveraging the advantages of highly sensitive, label-free, real-time, multiplexed detection within a single device. They are of high quality and have low fabrication costs due to their CMOS compatibility. However, although the sensor chips can be made as cheap disposable devices, an expensive and bulky high-resolution wavelength-tunable laser is required to accurately measure the resonance wavelength shift. To address this issue, we have developed a novel biosensor based on an electrical tracing-assisted dual-microring resonator sensor system on a SOI substrate, which allows the use of a low-cost broadband light source. By implementing broadband light source instead of a high-resolution wavelength tunable laser, the expected cost reduction for the instrument is minimum 20×. The dual-microring system comprises one microring resonator as a sensing element and another microring resonator integrated with an electrical controller as a tracing element. In this system, the resonance wavelength shift of the sensing microring caused by antigen–ligand bindings can be quantitatively monitored by measuring the electrical power applied to the tracing ring. A combination of silicon microring sensor technology and the use of a cost-effective broadband light source such as LED opens new opportunities for applications in portable POC devices that can be used at home, in general practitioners' offices or remote places where a central clinical lab is not accessible.

Acknowledgements

The author would like to acknowledge Edward Koh for providing technical supports. This work was supported by the Agency for Science Technology and Research (A*STAR) Joint Council Office (JCO) grant (JCOAG03_FG07_2009), Singapore.

Appendix A. Supporting information

Supplementary data associated with this article can be found in the online version at http://dx.doi.org/10.1016/j.bios.2013.02.002.

References

Bertrand, P., Jonas, A., Laschewsky, A., Legras, R., 2000. Macromolecular Rapid Communications 21 (7), 319–348.
Bohunicky, B., Mousa, S.A., 2011. Nanotechnology, Science and Applications 4, 1–10.
Byeon, J.-Y., Limpoco, F.T., Bailey, R.C., 2010. Langmuir 26 (19), 15430–15435.
Caruso, F., Niikura, K., Furlong, D.N., Okahata, Y., 1997. Langmuir 13 (13), 3422–3426.
Chilkoti, A., Tan, P.H., Stayton, P.S., 1995. Proceedings of the National Academy of Sciences 92 (5), 1754–1758.
Chua, J.H., Chee, R.-E., Agarwal, A., Wong, S.M., Zhang, G.-J., 2009. Analytical Chemistry 81 (15), 6266–6271.
De Vos, K., Bartolozzi, I., Schacht, E., Bienstman, P., Baets, R., 2007. Optics Express 15 (12), 7610–7615.
Encarnação, J.M., Baltazar, R., Stallinga, P., Ferrerira, G.N.M., 2009. Journal of Molecular Recognition 22 (2), 129–137.
Esteva, F.J., Cheli, C.D., Fritsche, H., Fornier, M., Slamon, D., Thiel, R.P., Luftner, D., Ghani, F., 2005. Brest Cancer Research 7 (4), R436–R443.
Gohring, J.T., Dale, P.S., Fan, X., 2010. Sensors and Actuators B: Chemical 146, 226–230.
Iqbal, M., Gleeson, M.A., Spaugh, B., Tybor, F., Gunn, W.G., Hochberg, M., Baehr-Jones, T., Bailey, R.C., Gunn, L.C., 2010. IEEE Journal on Selected Topics in Quantum Electronics 16 (3), 654–661.
Jung, L.S., Nelson, K.E., Stayton, P.S., Campbell, C.T., 2000. Langmuir 16 (24), 9421–9432.
Kirk, J.T., Fridley, G.E., Chamberlain, J.W., Chrsitensen, E.D., Hochberg, M., Ratner, D.M., 2011. Lab on a Chip 11 (7), 1372–1377.
Lin, S., Lee, A.S.-Y., Lin, C.-C., Lee, C.-K., 2006. Current Proteomics 3, 271–282.
McClellan, M.S., Domier, L.L., Bailey, R.C., 2012. Biosensors and Bioelectronics 31 (1), 388–392.
Park, M.K., Kee, J.S., Quah, J.Y., Netto, V., Song, J., Qing, F., La Fosse, E.M., Lo, G.-Q., 2013. Sensors and Actuators B: Chemical 176 552–259.
Pathirana, S.T., Barbaree, J., Chin, B.A., Hartell, M.G., Neely, W.C., Vodyanoy, V., 2000. Biosensors and Bioelectronics 15 (3–4), 135–141.
Pérez-Luna, V.H., O'Brien, M.J., Opperman, K.A., Hampton, P.D., López, G.P., Klumb, L.A., Stayton, P.S., 1999. Journal of the American Chemical Society 121 (27), 6469–6478.
Qavi, A.J., Bailey, R.C., 2010. Angewandte Chemie International Edition 49 (27), 4608–4611.
Qavi, A.J., Kindt, J.T., Gleeson, M.A., Bailey, R.C., 2011a. Analytical Chemistry 83 (15), 5949–5956.
Qavi, A.J., Mysz, T.M., Bailey, R.C., 2011b. Analytical Chemistry 83 (17), 6827–6833.
Rasooly, A., Jacobson, J., 2006. Biosensors and Bioelectronics 21 (10), 1851–1858.
Scheler, O., Kindt, J.T., Qavi, A.J., Kaplinski, L., Glynn, B., Barry, T., Kurg, A., Bailey, R.C., 2012. Biosensors and Bioelectronics 36 (1), 56–61.
Song, J., Fang, Q., Tao, S.H., Liow, T.-Y., Yu, M.B., Lo, G.Q., Kwong, D.-L., 2008. Optics Express 16 (20), 15304–15311.
Song, J., Luo, X., Tu., X., Park, M.K., Kee, J.S., Zhang, H., Yu, M., Lo, G.-Q., Kwong, D.-L., 2012. Optics Express 20 (4), 4189–4197.
Song, J., Fang, Q., Luo, X., Cai, H., Liow, T.-Y., Yu, M.B., Lo, G.Q., Kwong, D.-L., 2011. Optics Express 19 (12), 11220–11227.
Soper, S.A., Brown, K., Ellington, A., et al., 2006. Biosensors and Bioelectronics 21 (10), 1932–1942.
Spinke, J., Liley, M., Guder, H.-J., Angermaier, L., Knoll, W., 1993. Langmuir 9 (7), 1821–1825.
Taillaert, D., Laere, F.V., Ayre, M.W., Bogaerts, W., Thourhout, D.V., Bienstman, P., Beats, R., 2006. Japanese Journal of Applied Physics 45, 6071–6088.
Washburn, A.L., Gunn, L.C., Bailey, R.C., 2009. Analytical Chemistry 81 (22), 9499–9506.
Washburn, A.L., Luchansky, M.S., Bowman, A.L., Bailey, R.C., 2010. Analytical Chemistry 82 (1), 69–72.
Zimmermann, L., Tekin, T., Schroeder, H., Dumon, P., Bogaerts, W., 2008. IEEE LEOS Newsletter 22 (6), 4–14.